THE AMERICAN SOCIETY OF MECHANICAL ENGINEERS
Three Park Avenue, New York, N.Y. 10016-5990

99-GT-338

NDN-AXISYMMETRIC TURBINE END WALL DESIGN: Part II EXPERIMENTAL VALIDATION

J. C. Hartland, D. G. Gregory-Smith.
University of Durham, Durham, UK

N. W. Harvey, M. G. Rose.
Rolls-Royce plc, Derby, UK

ABSTRACT

The Durham Linear Cascade has been redesigned with the non-axisymmetric profiled end wall described in the first part of this paper, with the aim of reducing the effects of secondary flow. The design intent was to reduce the passage vortex strength and to produce a more uniform exit flow angle profile in the radial direction with less over turning at the wall. The new end wall has been tested in the linear cascade and a comprehensive set of measurements taken. These include traverses of the flow field at a number of axial planes and surface static pressure distributions on the end wall. Detailed comparisons have been made with the CFD design predictions, and also for the results with a planar end wall. In this way an improved understanding of the effects of end wall profiling has been obtained.

The experimental results generally agree with the design predictions, showing a reduction in the strength of the secondary flow at the exit and a more uniform flow angle profile. In a turbine stage these effects would be expected to improve the performance of any downstream blade row. There is also a reduction in the overall loss, which was not given by the CFD design predictions. Areas where there are discrepancies between the CFD calculations and measurement are likely to be due to the turbulence model used.

Conclusions for how the three-dimensional linear design system should be used to define end wall geometries for improved turbine performance are presented.

NOTATION

C_{ax}	Axial chord
C_p	(Upstream-Local) Static Pressure Coefficient.
C_{p0}	(Upstream-Local) Total Pressure Coefficient.
C_{ske}	Secondary Kinetic Energy Coefficient
V_{ex}	Nominal exit velocity
	Coefficients are made dimensionless by inlet velocity

INTRODUCTION

Turning the sheared flow due to the hub or casing boundary layers at inlet to a blade row causes secondary flows to be produced. In essence, the cross passage pressure gradient set up by the mainstream flow sweeps the low momentum boundary fluid from pressure to suction surface on the end-wall, with a compensating counter flow at a distance from the wall. Other phenomena are associated with secondary flow, which has been studied extensively. A comprehensive review was made by Sieverding (1985). The secondary flow gives rise to increased loss within the blade row and produces a non-uniform flow at exit which may cause extra loss in succeeding blade rows.

Part I of these papers describes the design of a non-axisymmetric end wall profile to counteract the secondary flow. By introducing curvature on the end wall the static pressure field can be modified, thus affecting the secondary flow. The idea of end wall profiling to reduce secondary flows is not new and Part I reviews some of the literature over the past four decades. However the recent advances in computational techniques has allowed the development of design techniques to optimise the three-dimensional shape of an end wall to reduce the effects of secondary flows.

This paper describes the experimental testing of the end wall profile whose design was described in Part I. The immediate predecessor to this work was that of Rose (1994) who suggested a design of the end wall for a nozzle guide vane to reduce the pressure non-uniformity at the platform trailing edge, as a means of reducing disc cooling leakage flow. His design was modified for a rotor blade which is used in the large-scale low speed cascade at Durham University. This work was reported by Hartland et al. (1998), who showed that the designed reduction in pressure non-uniformity was achieved very well, and that there was some effect on the secondary flow as was expected. A simple and quick method for machining an arbitrary end wall profile from polyurethane foam had been

Presented at the International Gas Turbine & Aeroengine Congress & Exhibition
Indianapolis, Indiana — June 7–June 10, 1999
This paper has been accepted for publication in the Transactions of the ASME
Discussion of it will be accepted at ASME Headquarters until September 30, 1999

evolved. Thus it was a relatively straightforward task to take the profile co-ordinates of the new end wall from the design data and manufacture it for testing in the cascade.

EXPERIMENTS

Durham Cascade

The cascade contains rotor blades of some 110° of turning; similar to those of a high pressure axial flow turbine. The cascade geometry is described by Gregory-Smith & Cleak (1992) and is illustrated in Figure 1. The blading design details are given in Table 1.

There is an upstream turbulence grid to give high inlet turbulence as indicated in Table 2. There are three slots one axial chord upstream of the cascade, used to determine the inlet flow conditions, as described by Moore & Gregory-Smith (1995). There are also 11 traverse slots, one upstream, seven within the cascade and three downstream. The flow is low speed with the Reynolds Number less (about half) than that for a typical HP rotor blade and so the flow shows significant transitional effects as described by Moore and Gregory-Smith (1996).

Table 1: Cascade Design Data

Inlet Flow Angle	42.75°
Blade Exit Angle	-68.7°
Blade Axial Chord, C_{ax}	181 mm
Blade Half-Span	200 mm
Reynolds Number (C_{ax} & V_{ex})	4.0×10^5
Exit Mach Number	0.1

Table 2: Inlet Flow, One Axial Chord Upstream

Free Stream	
Inlet Angle	43.5°
Streamwise Turbulence Intensity	5.1%
Spanwise Turbulence Intensity	5.6%
Normal Turbulence Intensity	5.0%
Turbulent k.e. Coefficient	0.0083
Turbulent Dissipation Rate	32.6 m^2/s^3
Mixing Length Scale	9.4mm
End Wall Boundary Layer	
99% Thickness	40 mm
Displacement Thickness	2.8 mm
Momentum Thickness	2.3 mm
Shape Factor	1.22

Instrumentation

The instrumentation is described in some detail by Hartland et al. (1998), and only the most significant features are mentioned here. To measure the endwall pressure distributions, the existing planar endwall of the cascade (made from Perspex) had been fitted with pressure tappings (~0.8mm internal diameter). The profiled endwall was machined in sections from polyurethane foam and the sections were coated with Melamine varnish and sanded smooth to give a hard surface with a good finish. Pressure tapping locations were as for the planar wall. The pressure tappings are polythene tubes (~0.76mm internal diameter) set through the endwall and sanded off to give a smooth finish.

For the investigation of the flow field, measurements were made upstream at slot 1 (9% C_{ax} upstream of the leading edge, i.e. −109%), within the blade passage at slots 6 and 8, and at

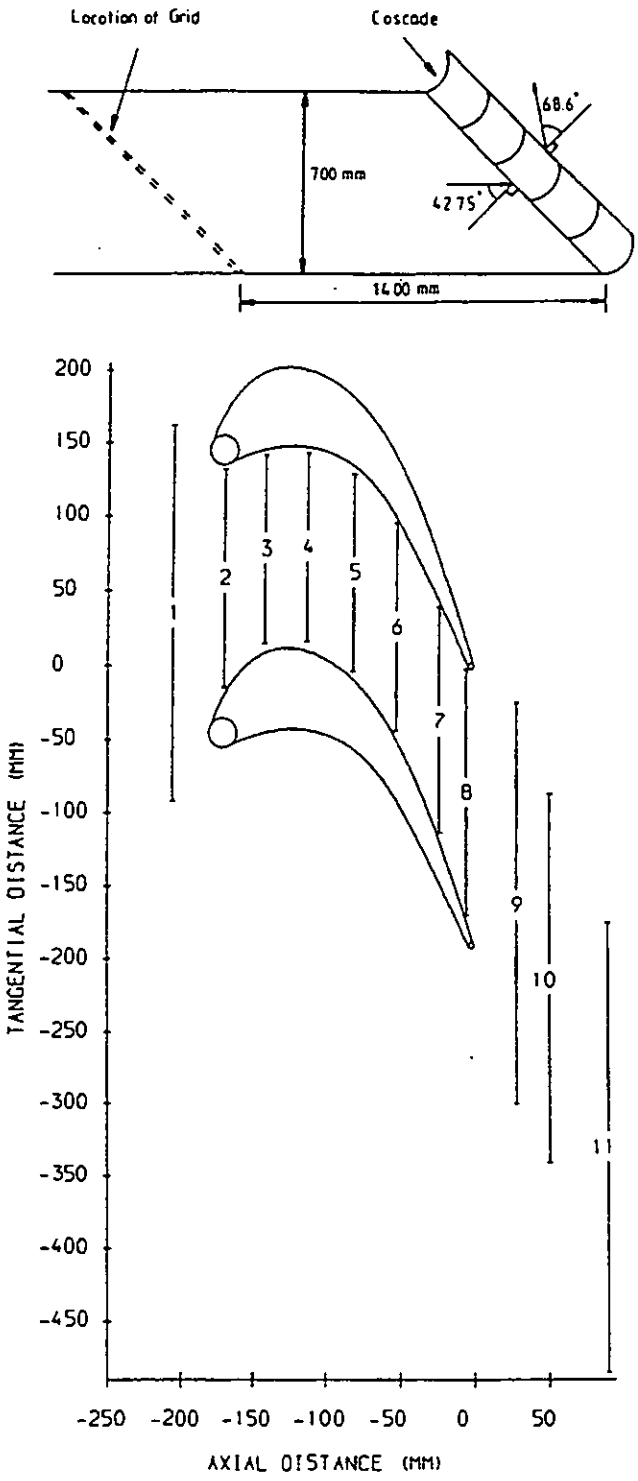

Figure 1: Cascade and Measurement Slots.

slot 10 (at -29%, -3% and 28% C_{ax} from the trailing edge respectively). A 5-holed cobra type probe was used to measure velocities and total pressure. These traverses were carried out with the profiled end wall in position, but also with a plane end wall made from the polyurethane, to ensure that the

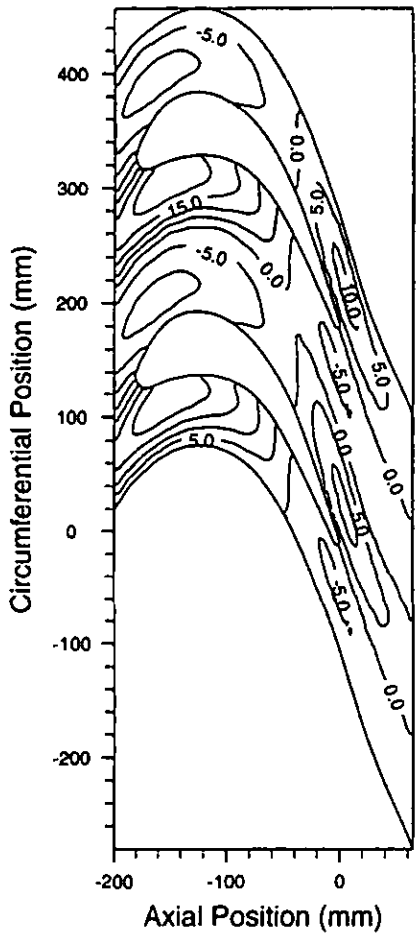

Figure 2: End Wall Height Contours

roughness difference between Perspex and the polyurethane did not affect the results.

Flow visualisation was carried out on the end walls using fluorescent dye in diesel oil.

RESULTS

Static Pressures

The shape of the end wall is described in Part I, and illustrated in Figure 2. It can be seen that the profiling extends upstream of the cascade, so that by the leading edge there is a significant variation in height across the pitch. There is a high region near the pressure surface, giving convex curvature so lowering the pressure, and a low region near the suction surface with concave curvature raising the pressure there. The contour levels are in millimetres, so the maximum height near the pressure surface is between 20mm and 25mm, and the minimum near the suction surface between –10mm and -15mm. In the design, a limitation in end wall perturbation was set at 25% of axial chord, i.e. 45mm.

Figure 3 shows the end wall static pressures for both the CFD and the experiments for the plane and profiled end walls. The contours are of static pressure coefficient, C_p, defined as the (upstream - local static pressure)/upstream dynamic pressure. The effect of the profiling on the pressure distribution in the early part of the passage seems to be rather more evident in the experimental than the CFD results. If the -1.0 contour is followed, it leaves the pressure surface at about -30mm axial position for both walls. For the planar wall it goes across the plotting area, leaving it at 195mm circumferential position, and coming back at 165mm to meet the suction surface just downstream of the leading edge. However for the profiled wall it curves round and meets the suction surface much further downstream, at about -150mm axial position. Thus near the suction surface, the pressure has been raised significantly. The effects of curvature on the static pressure magnitude are much greater near the suction surface because the velocity is higher there. The CFD results show the same effects but not so clearly.

Figure 4 shows a static pressure plot around the blade profile for the CFD at the end wall and at 4.65% height (17mm). At the end wall the pressure has been reduced a little on the pressure surface up to 60% axial chord, with a more significant raising of the pressure on the suction surface up to 40% axial chord. The effects are similar, although reduced at 4.65% height, but here the higher pressure on the suction surface extends to about 80% axial chord. By 10% height (40mm), the differences are almost zero. Experimental plots corresponding to those of Figure 4 were not obtained because of the problem of the tappings having to vary in spanwise position, depending on the shape of the end wall.

Towards the exit of the passage, the CFD results in Figures 3 and 4 show a lowering of pressure near the suction surface due to the convex curvature there indicated by the hump in Figure 2. This feature, as was explained in Part I, gives rise to a strengthened counter vortex in the design, so reducing the over turning on the end wall downstream. The effect is also seen in the experimental static pressures (Figure 3), although not so clearly.

Traverse Results - Area Plots

A selection of the traverse results using the five-hole probe is made here; fuller details are given by Hartland (1999). Figure 5 shows the results at slot 6, -29% C_{ax}. The planar end wall secondary vectors show the passage vortex well formed and convected towards the corner of the suction surface and end wall. The vortex is convected by its 'image' in the end wall and then away from the end wall by its 'image' in the suction surface, as will be seen later. This process has been observed by other workers, e.g. Gregory-Smith & Graves (1983), who describe it in detail. The rate of convection and its final position downstream is an indication of the strength of the secondary flow. The profiled end wall vortex appears weaker and it is centred approximately mid-pitch. The over turning close to the end wall appears significantly less, and is due to the reduction of the cross passage pressure gradient in the earlier part of the passage as seen by the static pressures. The secondary kinetic energy overall is reduced by about 10% (see Figure 11 later). Also in Figure 5 are the contours of total pressure loss. These are expressed as a loss coefficient, C_{p0}, defined as (upstream - local total pressure) / (inlet dynamic pressure). With the planar end wall most of the inlet boundary layer has been convected towards the suction surface, forming a high loss region which develops into the loss core later. Due to the lower cross flow close to it, the profiled end wall shows less convection of the boundary layer, and a smaller high loss region near the suction surface.

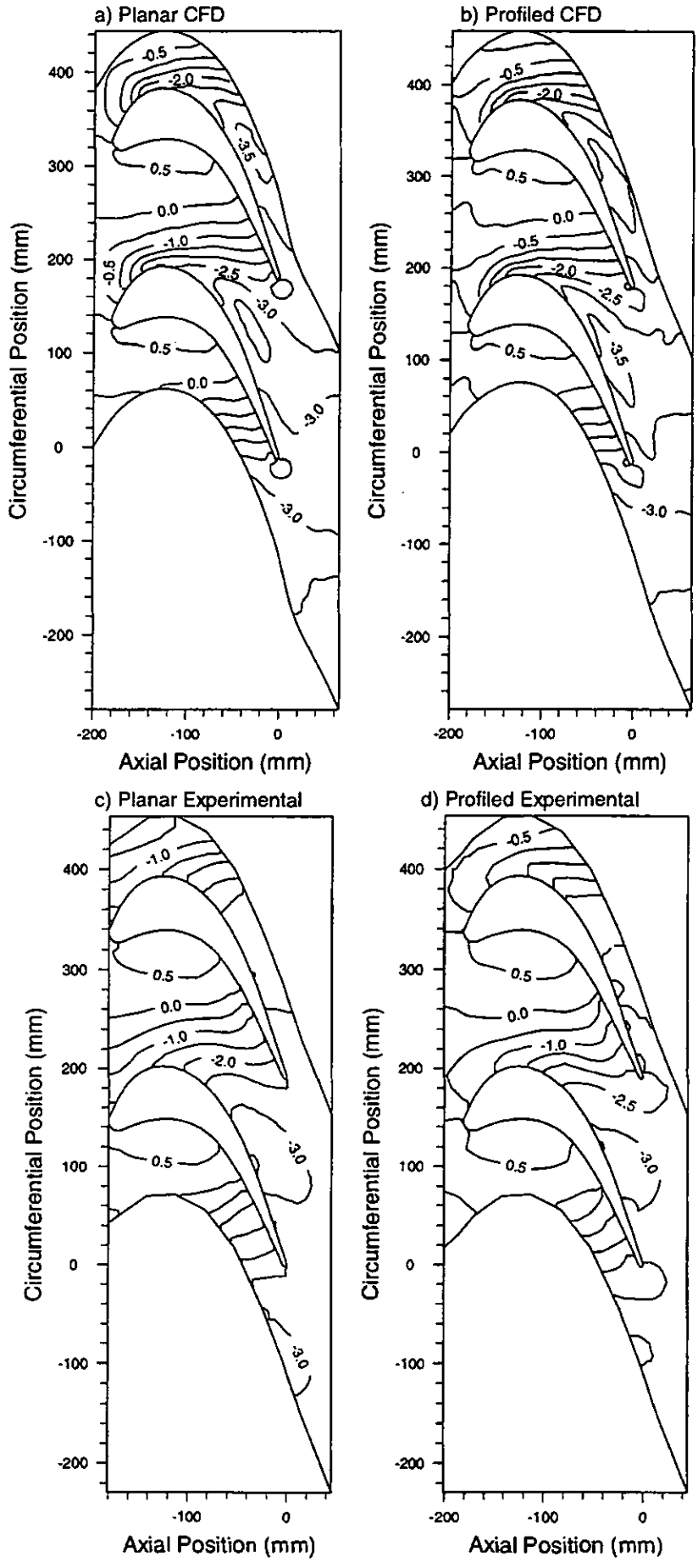

Figure 3: End Wall Static Pressures

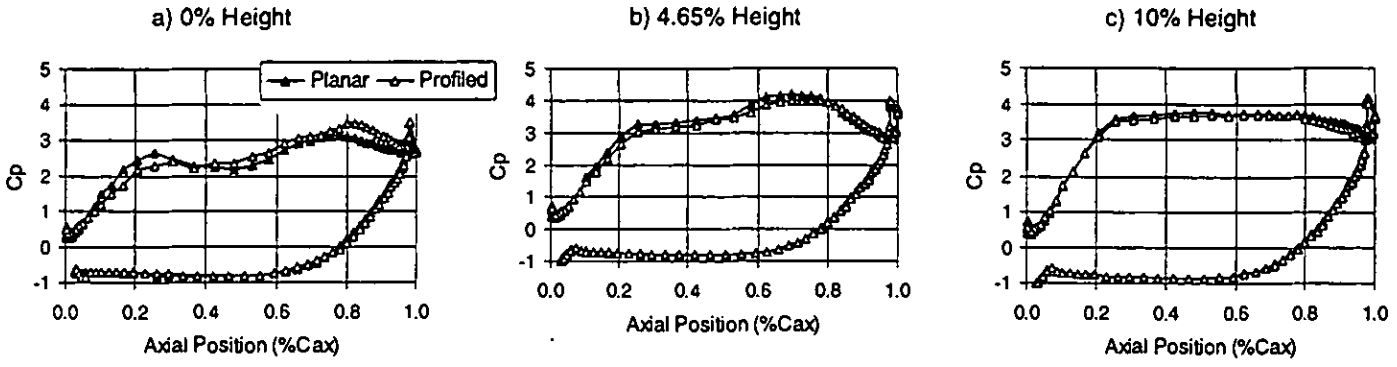

Figure 4: CFD Predictions of Blade Pressure Distributions

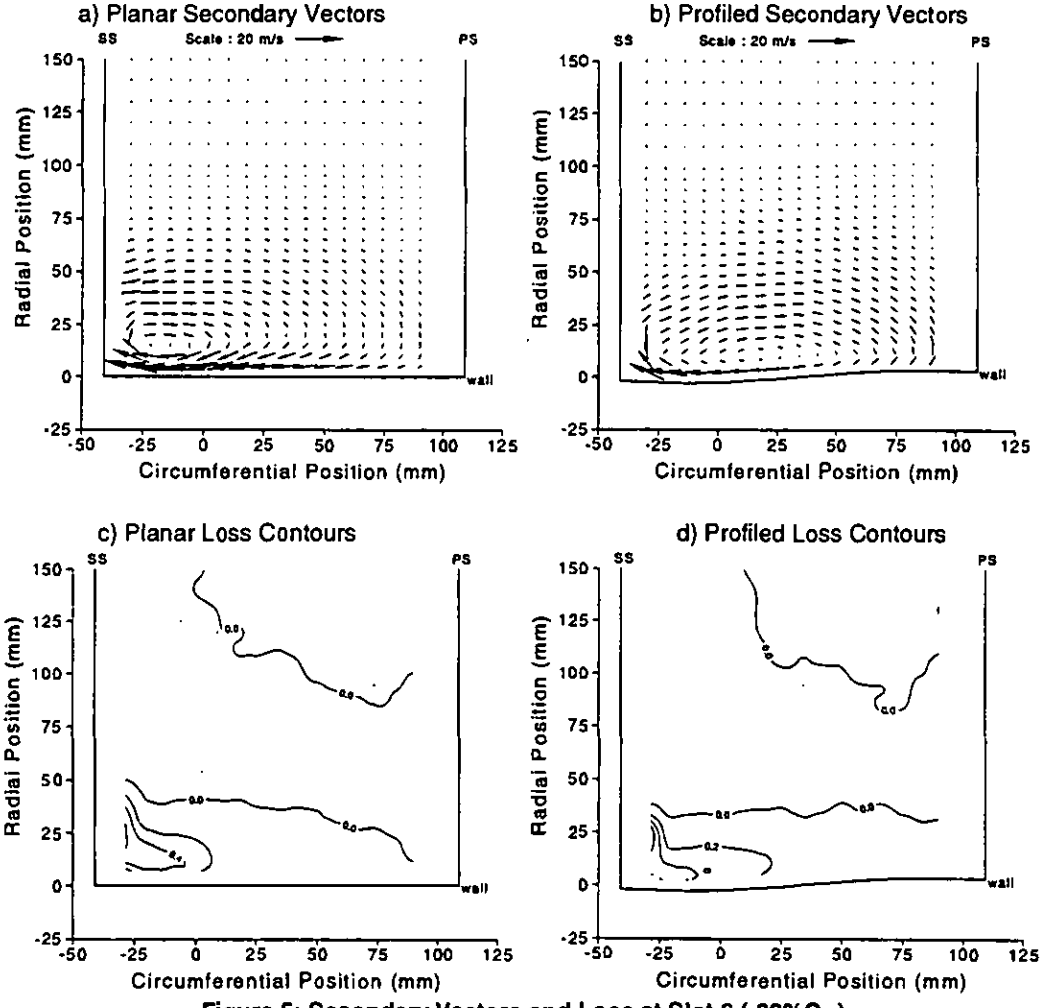

Figure 5: Secondary Vectors and Loss at Slot 6 (-29%C_{ax})

By slot 8 (-3% C_{ax}), just upstream of the trailing edge, for the planar wall the vortex has strengthened and has been convected away from the end wall, as shown in Figure 6. The profiled end wall shows a significantly weaker vortex, which has divided into two parts. The larger but weaker part is centred close to the wall and nearer the pressure surface, and the smaller part, which is more intense, is closer to the suction surface and further from the end wall. In the re-entrant corner between the suction surface and end wall, there is evidence of the strong counter vortex. The size of the probe prevented traversing closer into the corner. With respect to the loss contours, the plane end wall shows that the rolling up of the inlet boundary layer is well advanced, forming a loss core away from the end wall. The high-energy fluid has been convected close

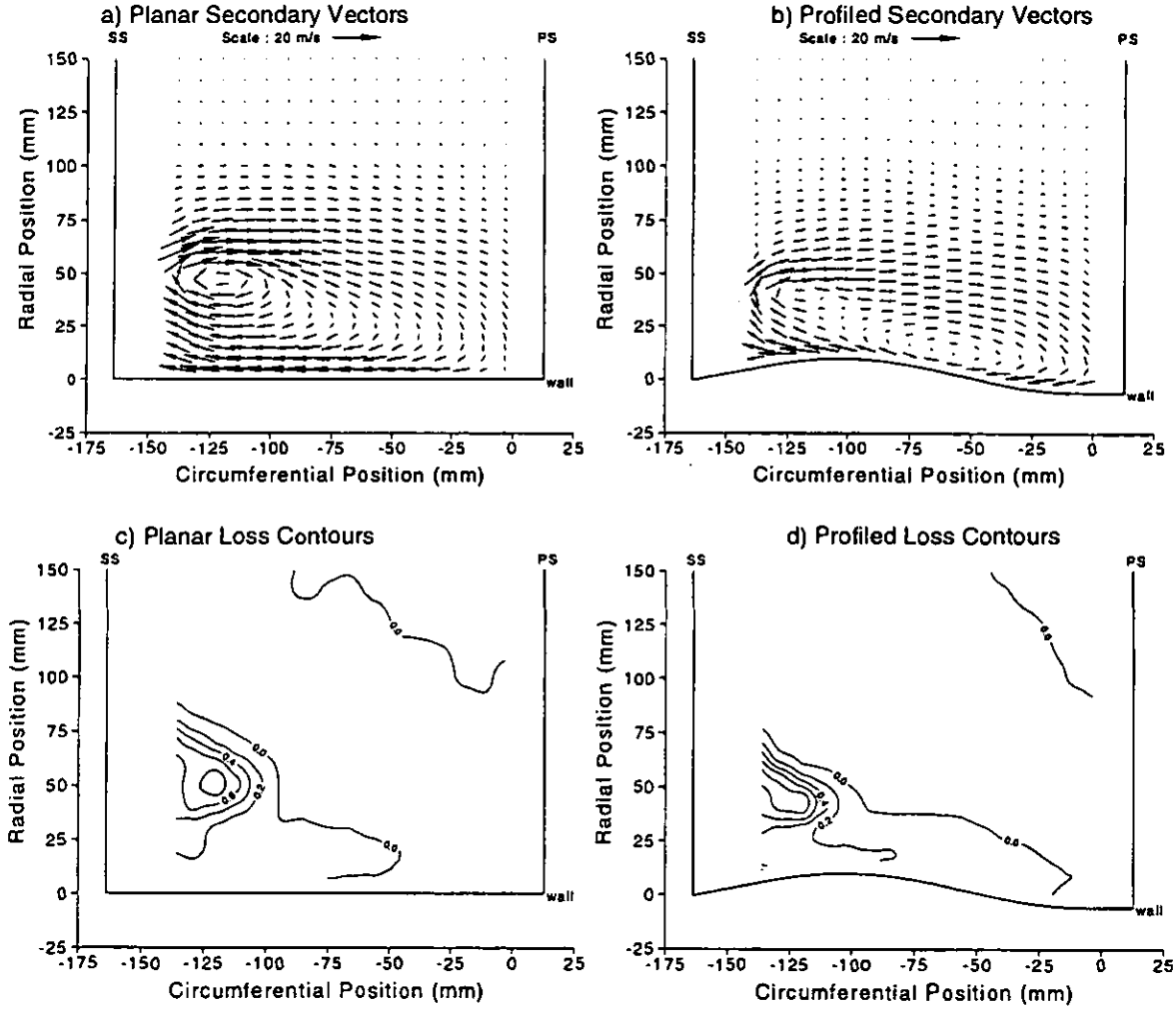

Figure 6: Secondary Vectors and Loss at Slot 8 (-3%C_{ax})

to the end wall over the pressure side half of the pitch. The profiled wall gives less rolling up of the boundary layer and convection of high-energy fluid, as a consequence of the lower secondary flows. The overall loss appears somewhat reduced.

The exit flow has been measured at slot 10 at 28% C_{ax} downstream. This is a little different from the exit plane which was used in the design process (29% C_{ax}). The secondary vectors as measured are shown in Figure 7, and the CFD predictions are shown in Figure 8 for comparison. The planar end wall shows the passage vortex (clockwise) further from the end wall, with a counter vortex (anti-clockwise) situated above it to the left, which stems from the trailing vorticity from the blade. On the end wall the small counter vortex is seen by low (zero) cross flow on the end wall. The profiled end wall has a less intense passage vortex, but the cross flow close to the end wall seems a little stronger, especially in the region on the hump close to the suction surface near the exit seen in Figure 2. The most significant difference with the profiled end wall is the strong counter vortex close to the end wall to the left of the hump, caused by the low pressure on its top. The CFD vectors (Figure 8) with the planar end wall shows the main features, but the vortex centre is not so far from the end wall as in the experiment. As Gregory-Smith (1995) has shown, this is quite common for CFD computations using a turbulence model which assumes turbulent flow through the blade passages, whereas in fact the flow on the blade surfaces and end wall is transitional (Moore & Gregory-Smith 1995). The CFD results for the profiled end wall again show the main features, and in particular the strong counter vortex. The loss contours in Figure 7 show that the end wall profile does not give the double loss peak of the loss core with the planar end wall, and the core is generally closer to the end wall. The distortion of the wake is less, and these features result from the generally lower secondary flow. The loss associated with the stronger counter vortex is a little greater as might be expected.

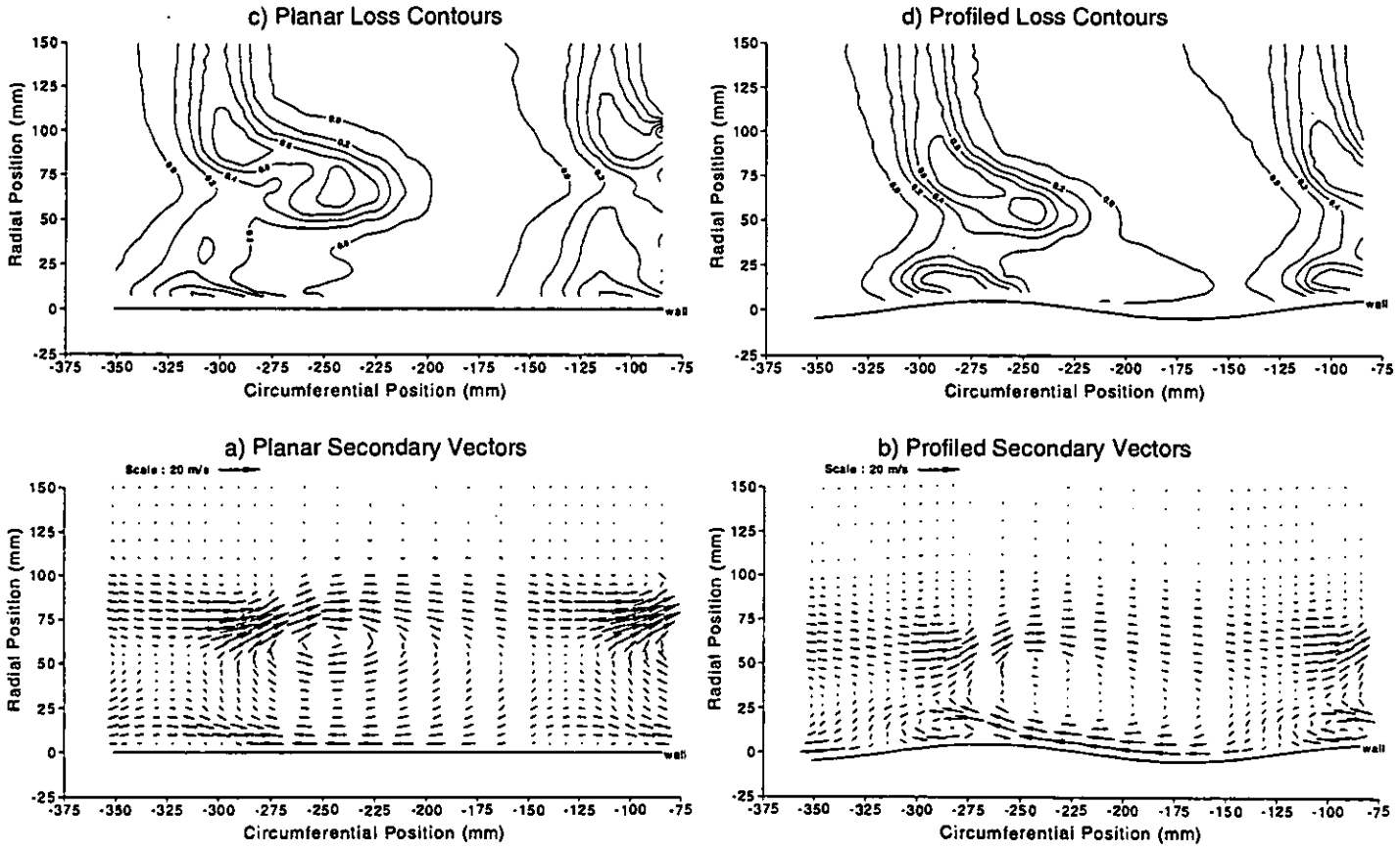

Figure 7: Secondary Vectors and Loss at Slot 10 (28%C_{ax})

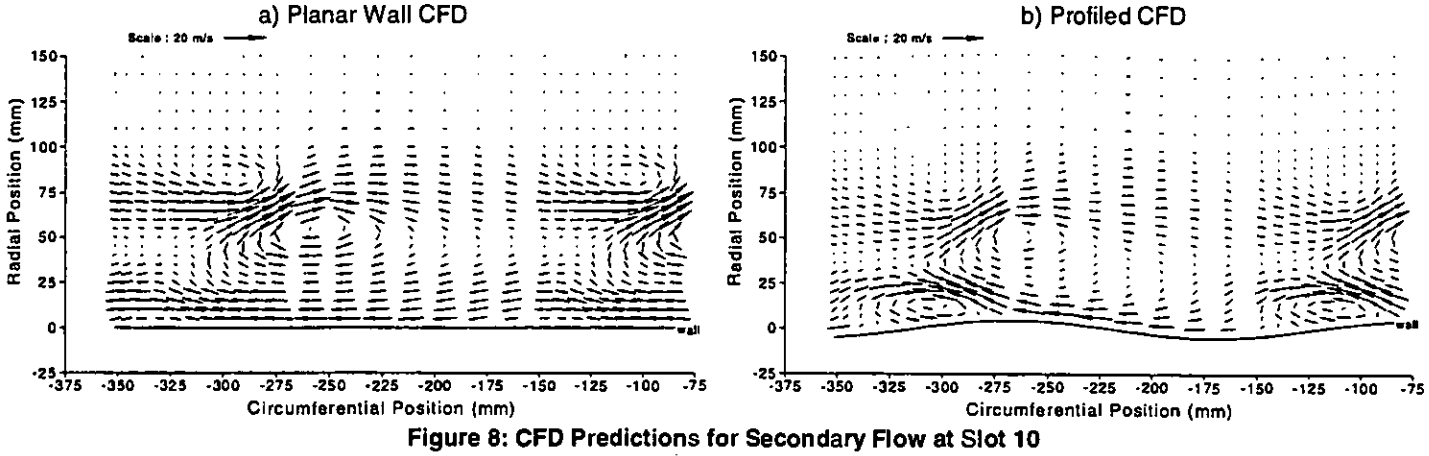

Figure 8: CFD Predictions for Secondary Flow at Slot 10

Pitch Averaged Results

The inlet flow profile is shown in Figure 9 as a total pressure loss coefficient. The two end walls have nearly identical flow, as would be expected, but there is a region of negative loss between 25mm and 125mm from the end wall. This was found to be due to the arrangement of the upstream turbulence grid, giving less pressure drop near the edge of the grid. This is important when the loss of the cascade is assessed, but to a first approximation the effect can be allowed for if 'net' loss is considered, i.e. the difference in loss between exit and inlet.

The legend is given for all the pitch averaged results, with planar end wall data signified by full symbols and profiled data by open ones. The experimental data are squares and the CFD data, triangles. Figure 10 shows the pitch averaged data at the downstream slot 10. The yaw angle shows an error at mid-span of about 1.5°, which may be due partly to a systematic angle error in the measurement. For the planar end wall the CFD

data has the under-turning peak closer to the end wall, although its value is accurate allowing for the mid-span difference. The profiled end wall gives a reduction in the under-turning peak of about 2° similar to that predicted by the CFD, but the peak is moved inwards by about 15mm, to the same position as the design CFD prediction. Inboard of the peak, the profiled end wall gives less over turning, both compared to the CFD and to the planar end wall, although the values on the wall are similar. In Figure 10b), the secondary kinetic energy coefficient, C_{ske}, defined as the local secondary kinetic energy divided by upstream mainstream kinetic energy, shows a large reduction in the peak with the profiled end wall. This is also shown by the CFD, although the peak values are slightly higher, and the movement inwards is not so great. Near the end wall, the profiled wall gives much more secondary kinetic energy, due to the strong counter vortex, and somewhat more than the CFD design.

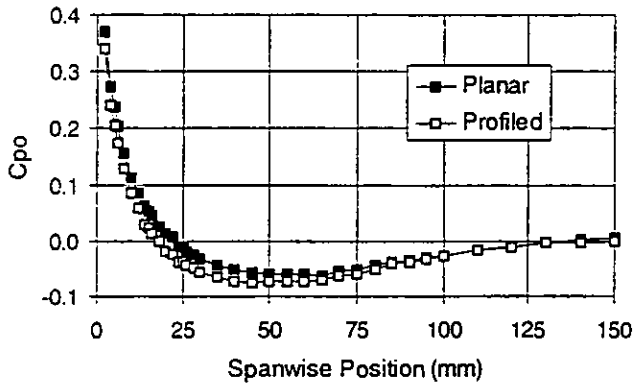

Figure 9: Pitch Averaged Loss Coefficient at Inlet

Figure 10c) shows that the pitch averaged loss peak is reduced significantly by the profiling, and is moved much closer to the end wall. The CFD shows only a slight reduction and not much movement inwards. Nearer in, the profiled end wall gives more loss (apart from the closest point to the end wall). This extra loss is mainly associated with the stronger counter vortex, which is also seen in the loss contours of Figure 7. However some of the "higher" loss is due to low energy fluid still being near to the end wall. Because of the delayed over turning less of this fluid has been convected into the loss core at this point.

The growth in secondary kinetic energy through the cascade is shown in Figure 11, where the mass weighted average across each traverse plane is plotted against axial position. The significant reduction with the profiled end wall is very evident, with the peak value at slot 8 (-3%) being reduced by about 40% for both the experiment and CFD. It may be noted that the CFD predicts slightly low values at slot 8, but high values at slot 10 (28%). This means the secondary velocities are being dissipated too slowly by the turbulence model, and this has been observed by other workers, e.g. Cleak & Gregory-Smith (1992).

A qualitative picture of the end wall flow is given by the flow visualisation, where dye has been injected through some of the pressure tappings, see Figure 12. It can be seen that the streaks at about 50% axial chord are displaced downstream for the profiled end wall due to the lower cross flow velocities. Towards exit, the cross flow seems as strong with the profiled end wall, but there is some evidence of the counter vortex near the suction surface trailing edge.

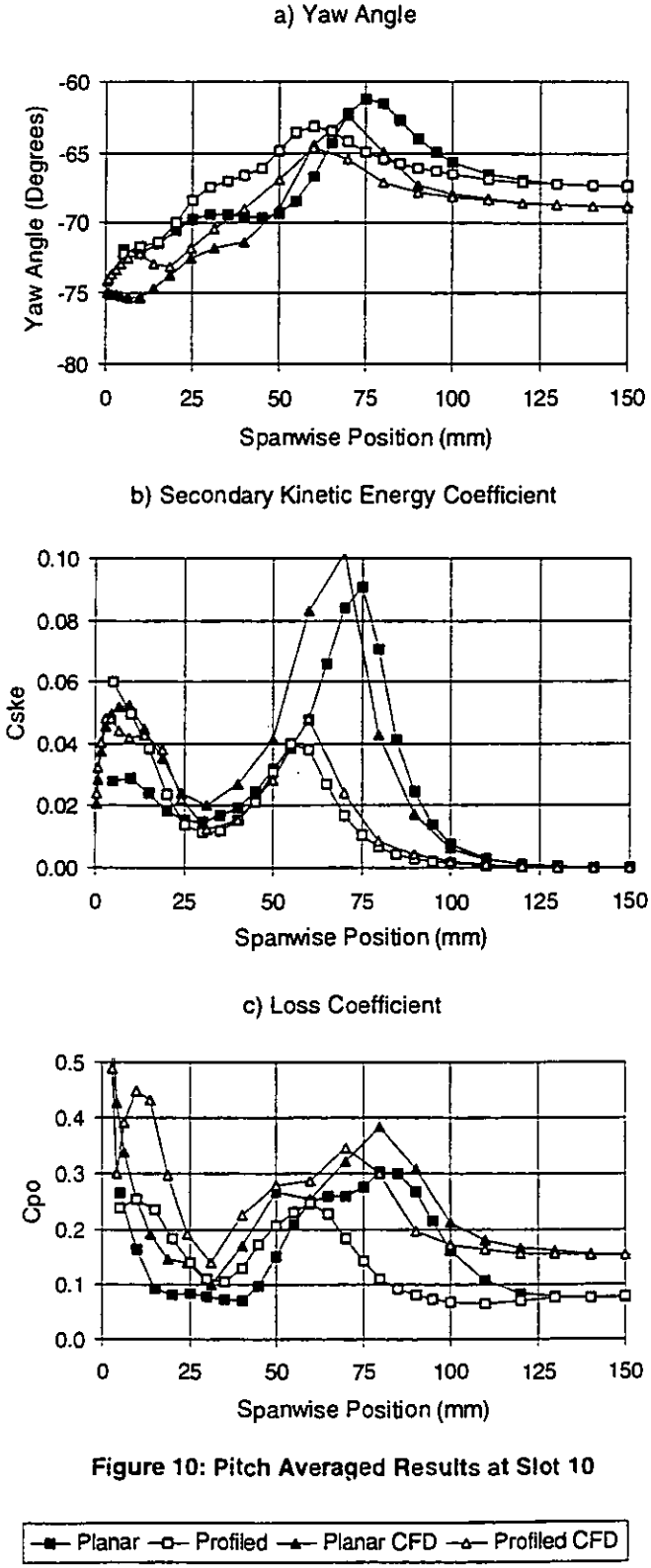

Figure 10: Pitch Averaged Results at Slot 10

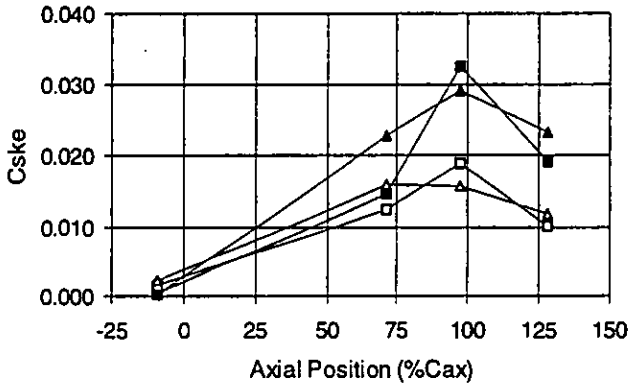

Figure 11: Growth of Secondary K.E. through the Cascade

Table 3 shows the net losses at slot 10. The mid-span loss is subtracted from the total loss to give the net secondary loss. It can be seen that the measured net total loss is reduced by 20% and the net secondary loss by 30%. The CFD losses show little change, and both giving total loss much too high due to high mid-span loss. Again this is a common error with CFD predictions because of the very fine grid that would be required for accurate profile loss prediction and the lack of any transition model in this transitional flow. Table 3 also shows the experimental mixed out losses, where the reductions with the profiled end wall are 15% in net total loss and 34% in secondary loss.

Table 3: Net Losses at Slot 10.

	C_{p0}		
	Full	Mid-Span	Secondary
Profiled	0.1108	0.0557	0.0551
Planar	0.1377	0.0598	0.0780
CFD Profiled	0.1937	0.1518	0.0419
CFD Planar	0.1926	0.1512	0.0414
	Mixed Out C_{p0}		
Profiled	0.1345	0.0709	0.0636
Planar	0.1588	0.0627	0.0961

DESIGN DISCUSSION

Overall the experiments largely confirm the design predictions for static pressure on the end wall. This is to be expected, because the static pressure distribution is largely due to the inviscid flow field, and modern CFD techniques should predict this well. Errors are only likely to arise if there are separations or large boundary layer growth, when the turbulence model is likely to perform poorly.

The traverse results also confirm the design reduction in secondary flow. In fact the experimental results seem to produce rather more improvement than the design predictions, with more general reduction in the passage vortex. This appears to be due to the slightly larger decrease in cross passage pressure difference observed in the experiments. The experiments confirm the much stronger corner counter vortex which was part of the design. Again, since the production of secondary flow from a sheared flow upstream is an inviscid effect, it is expected that the CFD should give good predictions.

Figure 12 EndWall Flow Visualisation

However, some of the details will be affected by the generation of loss (and hence shear) within the passage, and so the turbulence model may cause some error, but this should be small.

Where an unexpected benefit arises is the significant reduction observed in net loss across the cascade. The design was aimed primarily at reducing over- and under-turning at exit, with the object of improving the performance of a succeeding blade row. However the significant reduction of secondary flow has resulted in a reduction in loss. This intuitively might be expected due to lower scraping velocities on the end wall and suction surface from the passage vortex, and reduced mixing loss from the secondary velocities. The CFD predicts the secondary kinetic energy well, but the mixing length turbulence model is not adequate to translate this into accurate losses. The modelling required to improve on this is not clear, however. Moore and Gregory-Smith (1996) found that for the code used in this design, a k-e turbulence model performed rather worse than a mixing length model, especially if laminar and transitional regions are allowed for in the latter. More work in this area is needed.

The strong counter vortex is a source of extra loss as expected from the design, see Figures 10 and 7. It appears likely that the hump near the suction surface at exit, which causes this vortex, may not be desirable, since it also induces over turning flow on its other side (Figure 7 vectors). In the design the counter vortex was calculated to improve over turning at the wall. Its specific effect on whirl angle cannot be determined from the measurements directly, although the earlier slot traverses show reduced over turning (stemming from the reduced cross passage pressure difference) in the earlier part of the passage. If in fact this strong counter vortex is not necessary to reduce the over turning on the end wall, then it could be omitted resulting in an even larger reduction in loss.

CONCLUSION

This paper has tested experimentally a profiled end wall designed to reduce secondary flows. The following points may be concluded.

a) The static pressure field agrees well with the design prediction, and in fact seems to show a greater reduction in cross passage pressure difference in the early part of the passage than that for the design.
b) The resulting secondary flows are significantly reduced in the earlier part of the passage, and this reduction is convected downstream to give reduced secondary flow at exit. The profiled end wall gives significantly less angle variation at exit.
c) A strong corner counter vortex is observed according to the design prediction.
d) The net reduction in secondary loss is significant - 30% at the downstream exit plane, 34% in mixed out terms.
e) If the strong corner counter vortex is not needed to reduce the over turning on the end wall, then greater loss reduction can be achieved if it is omitted.

From the whole investigation on end wall profiling covered by both Part I and Part II papers, the following conclusions may be drawn.

1. A new linear design tool has been successfully developed for the design of non-axisymmetric end walls.
2. A first design of profiled end wall has achieved significant reductions in exit whirl angle deviations, secondary kinetic energy and secondary loss.
3. Future designs, making use of the inverse mode of the design code, higher order harmonics of wall shape and larger perturbation amplitudes, will seek to further reduce secondary flow and loss.
4. Non-axisymmetric end wall profiling is a powerful new tool available to the turbomachinery designer, and is expected will come to be as widely used as aerofoil lean and skew in the future.

ACKNOWLEDGEMENT

This work has been carried out with the support of Rolls-Royce plc and the Defence Evaluation and research Agency (MoD and DTI), Pyestock. The authors would like to thank them for funding it and their permission to publish this paper.

REFERENCES

Cleak J.G.E., Gregory-Smith D.G., (1992). "Turbulence Modelling for Secondary Flow Prediction in a Turbine Cascade." *J. Turbomachinery:* ASME Paper 91-GT-57 Vol.114 No.3, pp.590-598.

Gregory-Smith D.G., (1995), "Calculations of the Secondary Flow in a Turbine Cascade." International Symposium on Computational Fluid Dynamics in Aeropropulsion, ASME International ME'95 Congress and Exposition, November

Gregory-Smith D.G., Cleak J.G.E., (1992). "Secondary Flow Measurements in a Turbine Cascade with High Inlet Turbulence." *J. Turbomachinery:* ASME Paper No. 90-GT-20, Vol.114 No.1, pp.173-183.

Gregory-Smith D.G., Graves C.P., (1983) "Secondary Flows and Losses in a Turbine Cascade" AGARD-CP351, Paper No.17.

Hartland J.C., (1999) PhD. Thesis University of Durham, *to be submitted.*

Hartland J.C., Gregory-Smith D.G., Rose M.G., (1998) "Non-axisymmetric End Wall Profiling in a Turbine Rotor Blade." ASME Paper 98-GT-525

Moore H., Gregory-Smith D.G., (1995) "Turbulence and Transition in Secondary Flows in a Turbine Cascade." AGARD-CP571, PEP *Loss Mechanisms and Unsteady Flows in Turbomachines,* Paper No. 8

Moore H., Gregory-Smith D.G., (1996) "Transition Effects on Secondary Flows in a Turbine Cascade." ASME Paper No. 96-GT-100

Rose, M.G., 1994. "Non-axisymmetric endwall profiling in the HP NGVs of an axial flow gas turbine." ASME Paper No. 94-GT-249

Sieverding C.H., (1985), "Recent Progress in the Understanding of Basic Aspects of Secondary Flows In Turbine Blade Passages." ASME, J. Eng. Gas Turbines and Power, Vol.107, pp.248-252.